catalysts

MDPI

Article

Immobilization of Pyrroloquinoline Quinone-Dependent Alcohol Dehydrogenase with a Polyion Complex and Redox Polymer for a Bioanode

Yuki Sakurada, Kouta Takeda, Hiroyuki Ohno and Nobuhumi Nakamura *

Department of Biotechnology and Life Science, Tokyo University of Agriculture and Technology, 2-24-16 Nakacho, Koganei, Tokyo 184-8588, Japan; yuki-s@st.go.tuat.ac.jp (Y.S.); kouta@go.tuat.ac.jp (K.T.); ohnoh@cc.tuat.ac.jp (H.O.)

* Correspondence: nobu1@cc.tuat.ac.jp; Tel.: +81-42-388-7482

Received: 28 August 2017; Accepted: 30 September 2017; Published: 3 October 2017

Abstract: A bioanode for ethanol oxidation was prepared by immobilizing the recombinant pyrroloquinoline quinone (PQQ)-dependent alcohol dehydrogenase from *Pseudomonas putida* KT 2440 (*Pp*ADH) with polyion complex (PIC) and redox polymer. The PIC based on poly-L-lysine (PLL) and poly-L-glutamic acid (PGA) was suitable for immobilizing *Pp*ADH on the electrode. *Pp*ADH was immobilized using only one redox polymer, aminoferrocene, which was attached to the PGA backbone (PGA-AmFc) on the electrode. The anodic current density at 0.6 V (vs. Ag/AgCl) was 22.6 $\mu A \cdot cm^{-2}$. However, when the number of the cycles was increased, the catalytic current drastically decreased. *Pp*ADH was immobilized using PGA-AmFc and PIC on the electrode. The anodic current density at 0.5 V (vs. Ag/AgCl) was 47.3 $\mu A \cdot cm^{-2}$, and the performance maintained 74% of the initial value after five cycles. This result indicated that the combination of PIC and PGA-AmFc was suitable for the immobilization of *Pp*ADH on the electrode. In addition, the long-term stability and catalytic current density were improved by using the large surface area afforded by the gold nanoparticles.

Keywords: biofuel cells; quinoproteins; pyrroloquinoline quinone; alcohol dehydrogenase; polyion complex; redox mediator; gold nanoparticles

1. Introduction

Enzymatic biofuel cells that have enzymes on their electrodes initiate the oxidation reactions of various biologically relevant substrates, such as saccharides and alcohols, as well as the reduction reaction of oxygen to convert chemical energy from the biofuels into electrical energy. They can operate at normal temperature and pressure, and under neutral conditions, because of the suitable redox reaction conditions of most enzymes, and these biofuel cells have simple designs consisting of an anode and a cathode. Usually, enzymes containing nicotinamide adenine dinucleotide (NAD), flavin adenine dinucleotide (FAD), and pyrroloquinoline quinone (PQQ) for the anode and multi copper-containing redox proteins for the cathode are used [1,2]. For enzymes containing FAD and PQQ, their prosthetic groups are tightly bound to the active site, and the addition of cofactors in the system is not required. They are widely used in bioelectrochemical devices [3–5]. The complete oxidation of a biofuel in an enzymatic biofuel cell resulted in an increased energy density [6]. However, full electrons were not abstracted from the biofuel, because of these enzymes' broad substrate selectivity. Many kinds of enzymes are required for the complete oxidation of a biofuel. It is desirable to minimize the number of enzymes to achieve efficient oxidation in biofuels [7,8]. Some enzymes containing PQQ can catalyze various substrates because of their broad substrate specificity [9,10]. Previously, we reported a novel recombinant PQQ-dependent alcohol dehydrogenase from *Pseudomonas putida* KT 2440 (*Pp*ADH) expressed with *Pichia pastoris* [11]. This enzyme can catalyze the two-step oxidation of

ethanol to acetic acid. *Pp*ADH can be applied for the efficient oxidation of ethanol in an enzymatic biofuel cell.

Some enzymes can be used as electrocatalysts for biofuel cells by inducing direct electron transfer (DET) [12]. When DET is limited by a nonconductive protein shell or sugar chain, redox mediators are usually used to improve the transportation of electrons between the active site and the electrodes [13,14]. The main immobilization approaches for enzymatic biofuel cells are physical adsorption, covalent attachment, and entrapment [15,16]. Physical adsorption involves physical immobilization based on van der Waal's forces and electrostatic interactions [17]. Covalent attachment is chemical immobilization based on covalent bonding between enzyme surfaces and electrodes [18]. DET is influenced by the orientation of the enzyme and the close contact between the active sites and the electrodes. In many cases, to achieve DET, selected adsorption and covalent attachment are used as approaches for immobilizing enzymes to electrodes. Entrapment is an easy method for immobilizing enzymes and mediators in three-dimensional matrices [19]. Unlike DET systems, since mediated electron transfer systems are necessary for immobilizing both the enzyme and the mediator, such systems provide a good approach for entrapping them onto the electrode surface.

Because it is critical to immobilize both the mediator and the enzyme on the electrode, entrapment is more effective than adsorption or covalent attachment. The main strategies for entrapment involve confining the enzyme and mediator within a polyion complex (PIC) or redox hydrogel. It is known that PICs based on cationic polymers and anionic polymers are some of the most readily available matrices [19]. Enzyme immobilization within a PIC on the electrode is beneficial for avoiding enzyme denaturization [20]. Mizutani et al. succeeded in developing an enzyme that was immobilized in PIC electrodes for lactate-biosensing for the first time [21]. Recently, PIC has been applied not only in biosensors but also in biofuel cells [22,23]. Sakai succeeded in fabricating a biofuel cell with a maximum power density of 1.45 $mW \cdot cm^{-2}$ by using a PIC [22]. PICs can be applied to various electrode materials, such as carbon felt [24]. Therefore, PICs have a high versatility and are expected to be able to be used for enzyme immobilization.

During immobilization within a redox hydrogel, the enzyme becomes complexed with a redox polymer that is crosslinked on the electrode [25,26]. Heller et al. reported a redox polymer hydrogel to fabricate bioelectrodes [27]. Since then, the redox polymer has been widely applied for constructing bioelectrodes. Cheong et al. succeeded in fabricating an enzymatic biofuel cell with a maximum power density of 2.18 $mW \cdot cm^{-2}$ by using osmium complexes attached to the polymer [28].

In this study, we demonstrated the immobilization of *Pp*ADH on electrodes using a PIC. Aminoferrocene (AmFc) was employed to shuttle electrons between *Pp*ADH and the electrode. It was possible to design a simple electrode in which the enzyme and the mediator were immobilized within the electrode using a PIC and redox polymer. Ferrocene derivates attached to the polymer backbone were used as mediators for the bioelectrodes [29]. It was expected that the polymer containing AmFc was able to mediate the transportation of electrons between *Pp*ADH and the electrode. We prepared a redox polymer (PGA-AmFc) in which the carboxyl groups of poly-L-glutamic acid (PGA) and the amino groups of AmFc were bonded. We then constructed the electrode with *Pp*ADH immobilized within the optimized PIC and PGA-AmFc.

2. Results and Discussion

2.1. Optimization of the Polyion Complex for Immobilizing PpADH on the Electrode

We prepared electrodes with immobilized *Pp*ADH using cationic polymers: poly(diallyldimethylammonium chloride) (PDDA), poly-L-lysine (PLL), and poly(allylamine) (PAAm) and anionic polymers; poly(sodium 4-styrenene sulfonate) (PSS), PGA, and polyacrylic acid (PAA) (Figure 1).

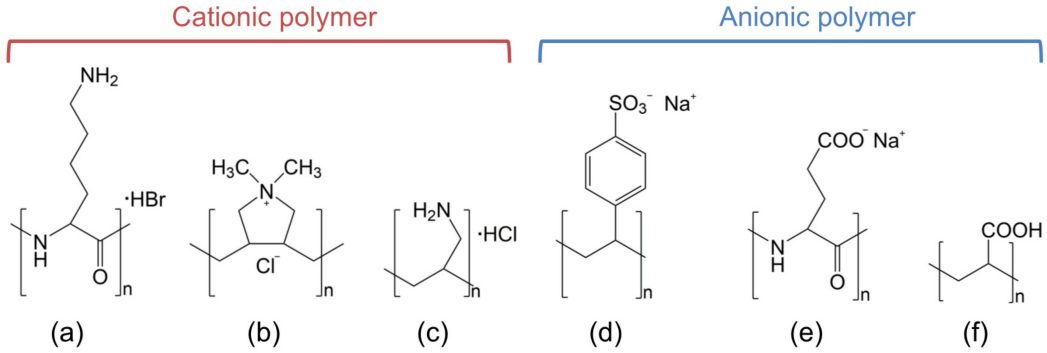

Figure 1. Schematic representation of the cationic polymers and anionic polymers used: poly-L-lysine hydrobromide (**a**), poly(diallyldimethylammonium chloride) (**b**), poly(allylamine hydrochloride) (**c**), poly(sodium 4-styrenesulfonate) (**d**), poly-L-glutamic acid sodium (**e**), and poly(acrylic acid) (**f**).

Nine types of PIC-modified electrodes were prepared; one of the cationic polymers, one of the anionic polymers and a *Pp*ADH solution were dropped onto a pretreated glassy carbon electrode. After drying for at least one hour at room temperature, the PIC-modified electrodes with *Pp*ADH were obtained, as schematically illustrated in Figure 2a. Figure 2b presents the cyclic voltammograms of the *Pp*ADH immobilized on the electrode with PLL and PGA in the absence and presence of ethanol containing AmFc.

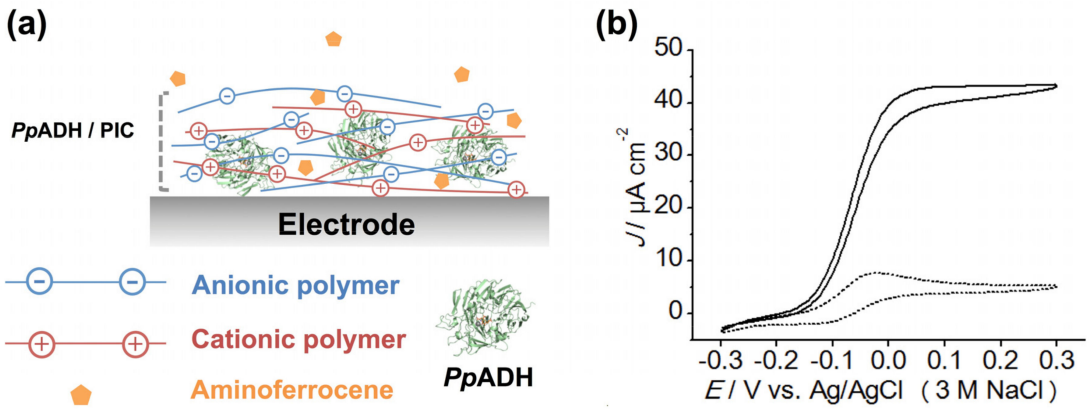

Figure 2. (**a**) Schematic illustration of *Pp*ADH-modified glassy carbon electrode with the polyion complex. (**b**) Cyclic voltammograms of the *Pp*ADH-modified glassy carbon electrode in 50 mM CHES (pH = 9.0) containing 30 mM ethylamine and 0.1 mM AmFc without a substrate (dotted line) and with 100 mM ethanol (solid line). The voltammograms were obtained at a scan rate of 10 mV·s^{-1}.

The cyclic voltammogram of AmFc exhibited a reversible response without ethanol. The midpoint potential of AmFc was estimated to be −0.08 V (vs. Ag/AgCl, at pH = 9.0). The catalytic current of the ethanol oxidation of *Pp*ADH was observed in this system (Figure 2b). The result indicated that the AmFc mediated the bioelectrocatalysis of the ethanol oxidation, and was similar to a previously reported voltammogram of a *Pp*ADH and AmFc diffusion system [11]. While the current density of a *Pp*ADH and AmFc diffusion system at 0.2 V (vs. Ag/AgCl, at pH = 9.0) was 18.8 μA·cm^{-2} [11], the current density of the *Pp*ADH immobilized on the electrode with PLL and PGA at 0.2 V (vs. Ag/AgCl, at pH = 9.0) was 43.1 μA·cm^{-2}. The result indicated that more of the reduced AmFc was generated on the electrode surface compared with the *Pp*ADH diffusion system.

Figure 3 shows the current densities of the electrodes at 0.3 V (vs. Ag/AgCl, at pH = 9.0). The catalytic current density on the PLL/*Pp*ADH/PGA electrode was 43.2 μA·cm^{-2} at 0.3 V (vs. Ag/AgCl, at pH = 9.0), which was the highest of all the electrodes. In contrast, the catalytic

current densities on the PDDA/*Pp*ADH/anionic polymer, PAAm/*Pp*ADH/anionic polymer, and PLL/*Pp*ADH/PSS electrodes were 12~19 μA·cm^{-2} at 0.3 V (vs. Ag/AgCl, at pH = 9.0). The catalytic current density on the PLL/*Pp*ADH/PAAm electrodes was 3.9 μA·cm^{-2} at 0.3 V (vs. Ag/AgCl at pH = 9.0), which was the lowest among all electrodes. When the number of cycles was increased, the catalytic currents of all electrodes decreased (Figure S1). This result suggested that *Pp*ADH and PIC were removed from the electrodes.

Cationic Polymer	PLL			PDDA			PAAm		
Anionic Polymer	PGA	PSS	PAA	PGA	PSS	PAA	PGA	PSS	PAA
Not Immersed (μA cm^{-2})	**43.2**	**14.9**	**3.9**	**19.3**	**14.3**	**15.9**	**17.5**	**12.3**	**14.7**
Immersed (μA cm^{-2})	23.6	2.8	2.6	0.6	1.8	5.2	3.1	2.1	1.4

Figure 3. Current densities of the glassy carbon electrodes modified with *Pp*ADH and PIC.

The electrodes were dipped in 50 mM CHES buffer (pH = 9.0) containing 30 mM ethylamine for an hour to remove the enzyme that was not immobilized. Figure 3 shows the current densities of the immersed electrodes at 0.3 V (vs. Ag/AgCl, at pH = 9.0). The catalytic current density on the immersed PLL/*Pp*ADH/PGA electrode was 23.6 μA·cm^{-2} at 0.3 V (vs. Ag/AgCl, at pH = 9.0), and it was the highest among all the immersed electrodes. In contrast, the catalytic current densities on the PDDA/*Pp*ADH/anionic polymer, PAAm/*Pp*ADH/anionic polymer, and PLL/*Pp*ADH/PSS electrode were 5 μA·cm^{-2} or less at 0.3 V (vs. Ag/AgCl, at pH = 9.0). These results indicate that the combination of PLL and PGA enhanced the immobilization of *Pp*ADH on the electrode and suggest that the reduction of the current density was largely due to enzyme desorption from the electrode.

2.2. Preparation of the Aminoferrocene-Attached Poly-L-glutamic Acid

To design biofuel cells more efficiently, we had to properly immobilize enzymes and mediators on the electrodes to improve electron communication between the enzymes and electrodes. The approach for immobilizing the enzyme and mediator was to entrap biocatalysts in the redox polymer. We prepared the redox polymer, PGA-AmFc, for *Pp*ADH. The carboxyl group of PGA was covalently linked to the free amine group of AmFc by an amide bond. After the reaction, unreacted AmFc was removed by ultrafiltration. Figure 4 shows the UV-visible spectrum of the PGA-AmFc.

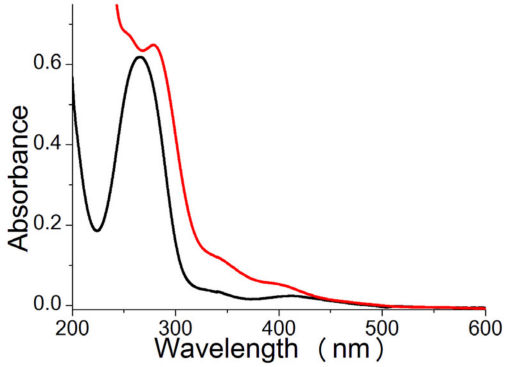

Figure 4. Absorption spectra of the AmFc (black) and PGA-AmFc (red) in deionized water.

The 260~280 nm bands of PGA-AmFc were attributed to the adsorption of peptide bonds in PGA. It is known that the UV-visible spectrum of ferrocene changes when the functional groups conjugate with ferrocene rings [30,31]. This is reasonable, since the 440 nm and 326 nm bands of ferrocene were attributed to metal-ring charge transfer, and it appears that the shifted transitions (412 nm and 344 nm bands) in AmFc were of the same type. These results suggest that the shifted transitions (407 nm and 348 nm bands) in PGA-AmFc were caused by metal-ring charge transfer.

Figure 5 shows cyclic voltammograms of PGA-AmFc. The cyclic voltammogram of PGA-AmFc exhibited reversible responses. The midpoint potential of PGA-AmFc was estimated to be 0.25 V (vs. Ag/AgCl, pH = 9.0). Compared to the midpoint potential of AmFc (−0.08 V vs. Ag/AgCl, pH = 9.0), the midpoint potential of PGA-AmFc shifted positively to 0.33 V (vs. Ag/AgCl). The redox potentials of the ferrocene derivatives indicated that the amount of electron withdrawing substituents increased, while the amount of electron donating substituents decreased [32]. This positive shift in the potential suggested that the electron donating effect of the amino groups of AmFc was weakened. These results indicated the attaching of AmFc to poly-L-glutamic acid.

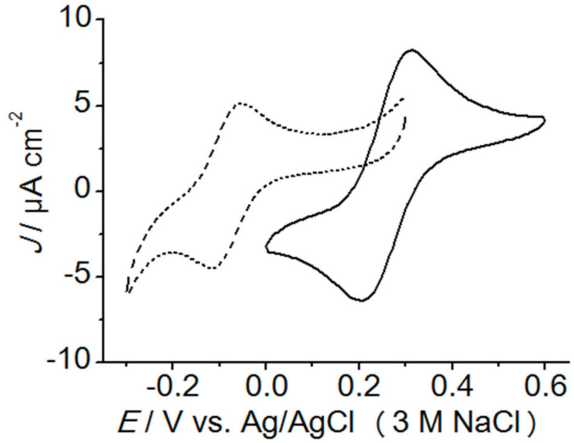

Figure 5. Cyclic voltammograms of the glassy carbon electrode in 50 mM CHES (pH = 9.0) containing 30 mM ethylamine with PGA-AmFc (solid line) and 0.5 mM AmFc (dotted line). The voltammograms were obtained at a scan rate of 10 mV·s^{-1} and an electrode area of 0.0707 cm^2.

The *Pp*ADH immobilized on the electrode with PLL and PGA-AmFc is shown as a schematic illustration in Figure 6a, and the cyclic voltammogram of *Pp*ADH immobilized on the electrode with PLL and PGA-AmFc in the presence of ethanol is shown in Figure 6b. The catalytic current of the ethanol oxidation of *Pp*ADH was observed. This result indicated the occurrence of PGA-AmFc-mediated bioelectrocatalysis during ethanol oxidation. However, while the catalytic current density on the electrode was 22.6 μA·cm^{-2} at 0.6 V (vs. Ag/AgCl, pH = 9.0), the catalytic current density during the fifth cycle decreased considerably to 22% (5.1 μA·cm^{-2}) (Figure 6b). When the number of cycles increased, the catalytic current decreased. This result suggested that *Pp*ADH and PGA-AmFc were removed from the electrode. The long-term stability of the *Pp*ADH-modified electrode using PGA-AmFc and PLL was low.

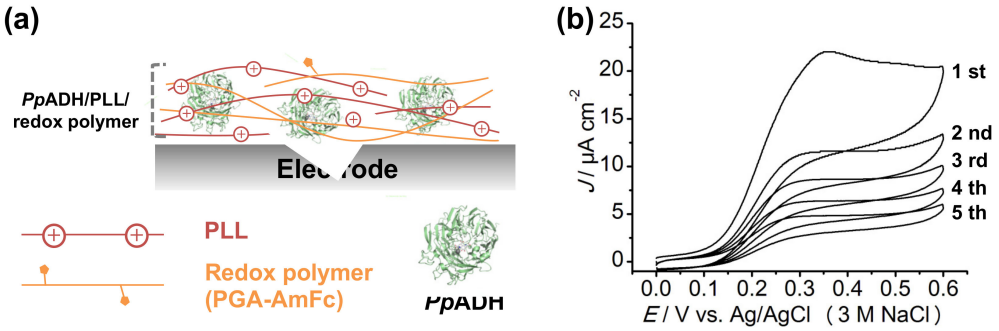

Figure 6. (**a**) Schematic illustration of the *Pp*ADH-modified glassy carbon electrode with the cationic polymer (PLL) and PGA-AmFc. (**b**) Cyclic voltammograms of the *Pp*ADH, PGA-AmFc and PLL-modified glassy carbon electrode from 1st scan to 5th scan in 50 mM CHES (pH = 9.0) containing 30 mM ethylamine and 100 mM ethanol. The voltammogram was obtained at a scan rate of 10 mV·s^{-1}.

2.3. Electrochemical Measurements of the *Pp*ADH-Modified Electrode Using PIC and PGA-AmFc

The combination of PLL and PGA enhanced the immobilization of *Pp*ADH on the electrode. We evaluated a simple electrode in which the enzyme and mediator were immobilized on the electrode with the PIC based on PLL and PGA and PGA-AmFc. PGA-AmFc and *Pp*ADH were successively placed on the glassy carbon electrode surfaces. The electrode was allowed to dry for at least one hour at room temperature. After drying, PLL and PGA were successively placed on the electrode. After drying for at least one hour at room temperature, the *Pp*ADH-modified electrode was obtained (GCE). The electrode structure of GCE is schematically illustrated in Figure 7a. Figure 7b shows the cyclic voltammogram of GCE.

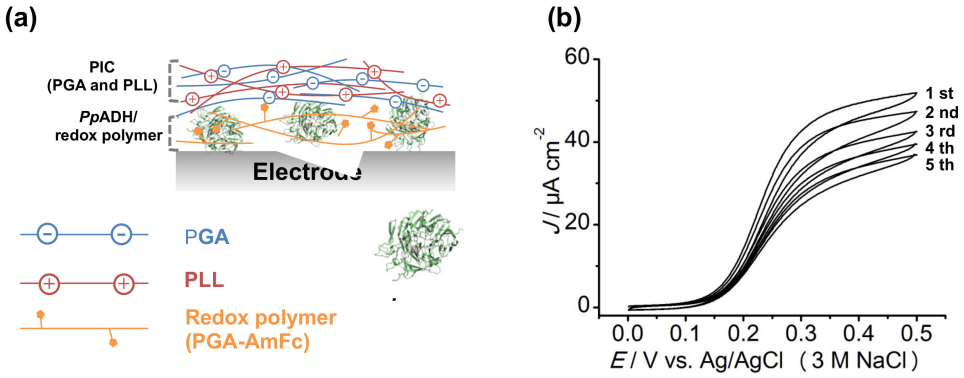

Figure 7. (**a**) Schematic illustration of the *Pp*ADH-modified GCE with the polyion complex and PGA-AmFc. (**b**) Cyclic voltammograms of the *Pp*ADH, PGA-AmFc, and polyion complex-modified GCE from 1st scan to 5th scan in 50 mM CHES (pH = 9.0) containing 30 mM ethylamine and 100 mM ethanol. The voltammograms were obtained at a scan rate of 10 $mV \cdot s^{-1}$.

The catalytic current of the ethanol oxidation of *Pp*ADH was observed. This result indicated that PGA-AmFc-mediated bioelectrocatalysis occurred during ethanol oxidation when it was combined with the PIC. The catalytic current density on the electrode was 47.3 $\mu A \cdot cm^{-2}$ at 0.5 V (vs. Ag/AgCl, pH = 9.0). The catalytic current density after five cycles slightly decreased to 73% (34.5 $\mu A \cdot cm^{-2}$) (Figure 7b). This result indicated that the combination of PIC based on PLL and PGA and PGA-AmFc was suitable for immobilizing *Pp*ADH on the electrode. The results suggest that the PIC layer prevented the desorption of *Pp*ADH and PGA-AmFc.

2.4. *Pp*ADH Modified Nanostructured Electrode Using PIC and PGA-AmFc

When constructing an electrode for an enzymatic biofuel cell, the important factors are the electrode design, such as the immobilized enzymes and mediators on the electrode, and the structure of the electrode interface to improve the performance of the enzymatic biofuel cell [33]. Various nanostructures, such as nanoparticles and nanocomposites, have been used to make bioelectrodes. The large surface area of these nanostructures leads to high enzyme loading, which can improve the power density of enzymatic biofuel cells. Electrodes can have a large effective surface area after adding a concentrated solution of AuNPs to the surface [34]. The Au surface can be chemically modified with thiols. Self-assembled monolayers (SAMs) of thiols are usually used to control the environment of the electrode surface. Here, we made SAM-modified AuNPs electrode surfaces on which PGA-AmFc and *Pp*ADH were successively placed. The electrode was allowed to dry for at least one hour at room temperature. After drying, PLL and PGA were successively placed on the electrode. After drying for at least one hour at room temperature, a *Pp*ADH-modified electrode was obtained (AuNPsE).

The electrode structure of AuNPsE is schematically illustrated in Figure 8a. The catalytic current of the AuNPs electrode without PGA-AmFc and *Pp*ADH was not observed (Figure S2). Figure 8b

shows the cyclic voltammogram of AuNPsE. The catalytic current of ethanol oxidation of *Pp*ADH was observed. The catalytic current density was 112.3 μA·cm^{-2} at 0.5 V (vs. Ag/AgCl, pH = 9.0), and it increased by 2.4 times compared with that of GCE. The results could be due to increasing the effective surface area of electrode per unit area. Figure 8c shows the relationship between the number of cycles and the current density in AuNPsE. The catalytic current density during the second cycle was 135 μA·cm^{-2} at 0.5 V (vs. Ag/AgCl, pH = 9.0). The catalytic current density at the 10th cycle decreased to 84% (113.7 μA·cm^{-2}) of the maximum catalytic density. The long-term stability of AuNPsE was improved compared to that of GCE. The results suggested that the PIC layer and nanostrcture of AuNPs prevented against the desorption of *Pp*ADH and PGA-AmFc.

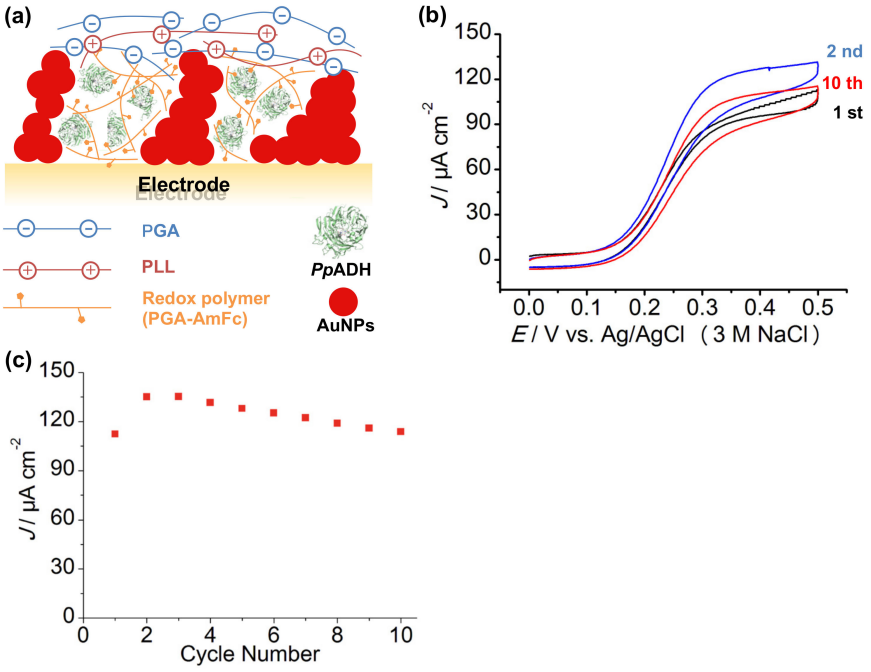

Figure 8. (**a**) Schematic illustration of the *Pp*ADH-modified AuNPsE with the polyion complex and PGA-AmFc. (**b**) Cyclic voltammograms of the *Pp*ADH and PGA-AmFc-modified AuNPsE at 1st scan (black), 2nd scan (blue), and 10th scan (red) in 50 mM CHES (pH = 9.0) containing 30 mM ethylamine and 100 mM ethanol. The voltammograms were obtained at a scan rate of 10 mV·s^{-1}. (**c**) Catalytic current densities of AuNPsE at 0.5 V vs. Ag/AgCl dependence on cycle number.

3. Materials and Methods

3.1. Materials

*Pp*ADH was heterologously expressed and purified as described previously. Poly-L-lysine hydrobromide (PLL) (molecular weight, 70,000-150,000), Poly(diallyldimethylammonium chloride) (PDDA) (molecular weight, 200,000), Poly(allylamine hydrochloride) (PAAm) (molecular weight, ~17,000), Poly(sodium 4-styrenesulfonate) (PSS) (molecular weight, 70,000), Poly-L-glutamic acid sodium (PGA) (molecular weight, 3000–15,000), Poly(acrylic acid) (PAA) (molecular weight, 25,000) (Sigma-Aldrich Japan G.K. (Tokyo, Japan)), aminoferrocene (AmFc), 1-ethyl-3-(3-dimethylaminopropyl)-carbodiimide hydrochloride (EDC), and 3-mercaptopropionic acid (MPA, from Dojindo, Japan) were purchased and used without further purification.

3.2. Preparation of PGA-AmFc

AmFc (1 mg) was dissolved in 1 mL of acetone and added dropwise to 9 mL of 4 mM HEPES (pH 7.0) with 35.5 mg of PGA and EDC (171.5 mg). The solution was mixed for 2 h at room temperature.

After the reaction, unreacted AmFc and EDC were removed using ultrafiltration. The total iron content in the PGA-AmFc was determined spectrophotometrically at 440 nm using a calibration curve for AmFc.

3.3. Electrode Preparation

The glassy carbon electrodes (3 mm in diameter) and gold electrodes (1.6 mm in diameter) were polished with alumina (particle size 3 μm:3 M Japan Limited, Tokyo, Japan) and chromium oxide (particle size 0.5 μm:3 M Japan Limited, Tokyo, Japan). This step was followed by ultrasonic cleaning and rinsing with deionized water.

20 μL of 10 mM Tris-HCl buffer solution (pH = 8.0) containing PGA-AmFc, *Pp*ADH (1 mg/mL), and 0.5 mM $CaCl_2$ was dropped on the glassy carbon electrode surface. The electrode was allowed to dry for at least one hour at room temperature. After drying, 10 μL of PLL (50 mM in monomer units) and 10 μL of PGA (50 mM in monomer unit) were dropped and mixed on the electrode. After drying for at least one hour at room temperature, the *Pp*ADH-modified electrodes were obtained (GCE).

The AuNPs were prepared following a procedure described by Frens [35]. Briefly, 12.5 mL of a 38.8 mM sodium citrate solution (Wako) was added to 125 mL of boiling 1.0 mM $HAuCl_4$ (Wako) with vigorous stirring. After the appearance of a deep red color, boiling and stirring were continued for 20 min. The solution was then allowed to cool to room temperature. The particle diameter of the AuNPs was estimated to be approximately 16 nm from the UV-vis spectrum of the solution.

The AuNP-modified electrodes were prepared following a procedure described by Murata [36]. Briefly, to increase the number of particles per volume, the AuNP solution was centrifuged (10,000× *g*, 30 min) in 1.5 mL Eppendorf tubes; then, 98% of the remaining supernatant volume was thrown away. Afterwards, 1 μL of the concentrated AuNPs were dropped onto the surface of the pretreated gold electrode, followed by drying in air. To increase the number of particles at the electrode, this procedure was repeated three times. Afterward, they were electrochemically cleaned in a 0.5 M H_2SO_4 solution using a scanning potential between −0.2 and 1.6 V (vs. Ag/AgCl) until a reproducible CV was obtained. The AuNP-modified electrodes were immersed in a 1 mM aqueous solution of MPA and left overnight at room temperature. The resulting electrodes were thoroughly rinsed with water to remove physically adsorbed thiol molecules.

5.6 μL of 10 mM Tris-HCl buffer solution (pH = 8.0) containing PGA-AmFc, *Pp*ADH (1 mg/mL), and 0.5 mM $CaCl_2$ was dropped on the AuNPs electrode surface. The electrode was allowed to dry for at least one hour at room temperature. After drying, 2.8 μL of PLL (50 mM in monomer units) and 2.8 μL of PGA (50 mM in monomer unit) were dropped and mixed on the electrode. After drying for at least one hour at room temperature, the *Pp*ADH-modified electrodes were obtained (AuNPsE).

3.4. Electrochemical Measurements

All electrochemical measurements were conducted using an ALS electrochemical analyzer 612 (BAS Inc., Tokyo, Japan). A conventional three-electrode cell was used, in which a platinum wire served as the counter electrode, and Ag/AgCl (3 M NaCl) served as the reference electrode. All redox potentials in this report are relative to the Ag/AgCl (3 M NaCl) electrode. Cyclic voltammetry was performed in 50 mM CHES buffer (pH = 9.0) containing 30 mM ethylamine and 100 mM ethanol at room temperature. The alcohol oxidation activity of *Pp*ADH was activated by amines as an activator in vitro assays with artificial electron acceptors [37]. The pH of the solution was close to the optimal pH for *Pp*ADH [11]. For all measurements, the scan rate and range were set to 10 $mV \cdot s^{-1}$.

4. Conclusions

The immobilization of *Pp*ADH on electrodes with PIC was optimized. PIC based on PLL and PGA was appropriate for *Pp*ADH. We fabricated AmFc modified redox polymer, which acted as a redox mediator to shuttle electrons between *Pp*ADH and the electrode. The use of PIC in combination of the redox polymer enables immobilization of *Pp*ADH on the electrode and its efficient electron

communication between enzyme and electrode. The AuNPs electrode fabricated *Pp*ADH with PIC and the redox polymer were shown to improve the catalytic current and long-term stability.

Supplementary Materials: The following are available online at www.mdpi.com/2073-4344/7/10/296/s1. Figure S1: Stability of the *Pp*ADH modified electrodes, and Figure S2: Cyclic voltammograms of the PGA and PLL modified AuNPs electrode.

Acknowledgments: This work was supported by a Grant-in-Aid for Young Scientists (B), JSPS KAKENHI Grant Number 17K17703 to Kouta Takeda.

Author Contributions: Y.S. and K.T. performed the experiments; Y.S., K.T., and N.N. analyzed the data; Y.S., K.T., N.N., and H.O. contributed reagents/materials/analysis tools; and Y.S., K.T., and N.N. wrote the paper.

Conflicts of Interest: The authors declare no conflict of interest.

References

1. Palmore, G.T.R.; Whitesides, G.M. Microbial and enzymatic biofuel cells. *ACS Symp. Ser.* **1994**, *566*, 271–290.
2. Shleev, S.; Tkac, J.; Christenson, A.; Ruzgas, T.; Yaropolov, A.I.; Whittaker, J.W.; Gorton, L. Direct electron transfer between copper-containing proteins and electrodes. *Biosens. Bioelectron.* **2005**, *20*, 2517–2554. [CrossRef] [PubMed]
3. Scherbahn, V.; Putze, M.T.; Dietzel, B.; Heinlein, T.; Schneider, J.J.; Lisdat, F. Biofuel cells based on direct enzyme-electrode contacts using PQQ-dependent glucose dehydrogenase/bilirubin oxidase and modified carbon nanotube materials. *Biosens. Bioelectron.* **2014**, *61*, 631–638. [CrossRef] [PubMed]
4. Neto, S.A.; Milton, R.D.; Hickey, D.P.; De Andrade, A.R.; Minteer, S.D. Membraneless enzymatic ethanol/O_2 fuel cell: Transitioning from an air-breathing Pt-based cathode to a bilirubin oxidase-based biocathode. *J. Power Sources* **2016**, *324*, 208–214. [CrossRef]
5. Tuurala, S.; Lau, C.; Atanassov, P.; Smolander, M.; Minteer, S.D. Characterization and stability study of immobilized PQQ-dependent aldose dehydrogenase bioanodes. *Electroanalysis* **2012**, *24*, 229–238. [CrossRef]
6. Palmore, G.T.R.; Bertschy, H.; Bergens, S.H.; Whitesides, G.M. A methanol/dioxygen biofuel cell that uses NAD^+-dependent dehydrogenases as catalysts: Application of an electro-enzymatic method to regenerate nicotinamide adenine dinucleotide at low overpotentials. *J. Electroanal. Chem.* **1998**, *443*, 155–161. [CrossRef]
7. Arechederra, R.L.; Minteer, S.D. Complete oxidation of glycerol in an enzymatic biofuel cell. *Fuel Cells.* **2009**, *9*, 63–69. [CrossRef]
8. Xu, S.; Minteer, S.D. Enzymatic biofuel cell for oxidation of glucose to CO_2. *ACS Catal.* **2012**, *2*, 91–94. [CrossRef]
9. Arechederra, R.L.; Treu, B.L.; Minteer, S.D. Development of glycerol/O_2 biofuel cell. *J. Power Sources.* **2007**, *173*, 156–161. [CrossRef]
10. Sakuta, R.; Takeda, K.; Igarashi, K.; Ohno, H.; Nakamura, N. Enzymes suitable for biorefinery to coproduce hexaric acids and electricity from hexuronic acids derived from biomass. *Energy Technol.* **2017**, *25*. [CrossRef]
11. Takeda, K.; Matsumura, H.; Ishida, T.; Samejima, M.; Igarashi, K.; Nakamura, N.; Ohno, H. The two-step electrochemical oxidation of alcohols using a novel recombinant PQQ alcohol dehydrogenase as a catalyst for a bioanode. *Bioelectrochemistry* **2013**, *94*, 75–78. [CrossRef] [PubMed]
12. Eddowes, M.J.; Hill, H.A.O. Novel method for investigation of electrochemistry of metalloproteins: Cytochrome c. *J. Chem. Soc. Chem. Commun.* **1977**, 771–772. [CrossRef]
13. Williams, D.L.; Doig, A.R., Jr.; Korosi, A. Electrochemical-enzymatic analysis of blood glucose and lactate. *Anal. Chem.* **1970**, *42*, 118–121. [CrossRef] [PubMed]
14. Kim, J.; Jia, H.F.; Wang, P. Challenges in biocatalysis for enzyme-based biofuel cells. *Biotechnol. Adv.* **2006**, *24*, 296–308. [CrossRef] [PubMed]
15. Yu, E.H.; Scott, K. Enzymatic biofuel cells-fabrication of enzyme electrodes. *Energies* **2010**, *3*, 23–42. [CrossRef]
16. Arya, S.K.; Datta, M.; Malhotra, B.D. Recent advances in cholesterol biosensor. *Biosens. Bioelectron.* **2008**, *23*, 1083–1100. [CrossRef] [PubMed]
17. Choi, M.M.F. Progress in enzyme-based biosensors using optical transducers. *Microchim. Acta* **2004**, *148*, 107–132. [CrossRef]
18. Sassolas, A.; Blum, L.J.; Leca-Bouvier, B.D. Immobilization strategies to develop enzymatic biosensors. *Biotechnol. Adv.* **2012**, *30*, 489–511. [CrossRef] [PubMed]

19. Yabuki, S. Polyelectrolyte complex membranes for immobilizing biomolecules, and their applications to bio-analysis. *Anal. Sci.* **2011**, *27*, 695–702. [CrossRef] [PubMed]
20. Katsuno, E.; Yabuuchi, N.; Komaba, S. Double-layered polyion complex for application to biosensing electrodes. *Electrochem. Commun.* **2014**, *47*, 88–91. [CrossRef]
21. Mizutani, F.; Yabuki, S.; Hirata, Y. Amperometric L-lactate-sensing electrode based on a polyion complex layer containing lactate oxidase. Application to serum and milk samples. *Anal. Chim. Acta* **1995**, *314*, 233–239. [CrossRef]
22. Sakai, H.; Nakagawa, T.; Tokita, Y.; Hatazawa, T.; Ikeda, T.; Tsujimura, S.; Kano, K. A high-power glucose/oxygen biofuel cell operating under quiescent conditions. *Energy Environ. Sci.* **2009**, *2*, 133–138. [CrossRef]
23. Komaba, S.; Mitsuhashi, T.; Shiraishi, S. Polyion complex nanocomposite electrode incorporating enzyme and carbon nanotube for biofuel cells. *Electrochemistry* **2008**, *76*, 55–58. [CrossRef]
24. Yabuki, S.; Hirata, Y. Enzyme and mediator-coadsorbed carbon felt electrode for electrochemical detection of glucose covered with polymer layers based on layer-by-layer technique. *Anal. Sci.* **2015**, *31*, 693–697. [CrossRef] [PubMed]
25. Hou, C.T.; Lang, Q.L.; Liu, A.H. Tailoring 1,4-naphthoquinone with electron-withdrawing group: Toward developing redox polymer and FAD-GDH based hydrogel bioanode for efficient electrocatalytic glucose oxidation. *Electrochim. Acta* **2016**, *211*, 663–670. [CrossRef]
26. Osman, M.H.; Shah, A.A.; Walsh, F.C. Recent progress and continuing challenges in bio-fuel cells. Part I: Enzymatic cells. *Biosens. Bioelectron.* **2011**, *26*, 3087–3102. [CrossRef] [PubMed]
27. Degani, Y.; Heller, A. Electrical communication between redox centers of glucose oxidase and electrodes via electrostatically and covalently bound redox polymers. *J. Am. Chem. Soc.* **1989**, *111*, 2357–2358. [CrossRef]
28. Kwon, C.H.; Lee, S.-H.; Choi, Y.-B.; Lee, J.A.; Kim, S.H.; Kim, H.-H.; Spinks, G.M.; Wallace, G.G.; Lima, M.D.; Kozlov, M.E.; et al. High-power biofuel cell textiles from woven biscrolled carbon nanotube yarns. *Nat. Commun.* **2014**, *5*, 3928. [CrossRef] [PubMed]
29. Hodak, J.; Etchenique, R.; Calvo, E.J.; Singhal, K.; Bartlett, P.N. Layer-by-layer self-assembly of glucose oxidase with a poly(allylamine)ferrocene redox mediator. *Langmuir* **1997**, *13*, 2708–2716. [CrossRef]
30. Little, W.F.; Clark, A.K. Ferrocenylazobenzenes. Resonance interaction of ferrocene with substrates. *J. Org. Chem.* **1960**, *25*, 1979–1982. [CrossRef]
31. Tarr, A.M.; Wiles, D.M. Electronic absorption spectra and photodecomposition of some substituted ferrocenes. *Can. J. Chem.* **1968**, *46*, 2725–2731. [CrossRef]
32. Kuwana, T.; Bublitz, D.E.; Hoh, G. Chronopotentiometric studies on the oxidation of ferrocene, ruthenocene, osmocene and some of their derivatives. *J. Am. Chem. Soc.* **1960**, *82*, 5811–5817. [CrossRef]
33. Barton, S.C.; Gallaway, J.; Atanassov, P. Enzymatic biofuel cells for implantable and microscale devices. *Chem. Rev.* **2004**, *104*, 4867–4886. [CrossRef] [PubMed]
34. Suzuki, M.; Murata, K.; Nakamura, N.; Ohno, H. The effect of particle size on the direct electron transfer reactions of metalloproteins using au nanoparticle-modified electrodes. *Electrochemistry* **2012**, *80*, 337–339. [CrossRef]
35. Frens, G. Controlled nucleation for the regulation of the particle size in monodisperse gold suspensions. *Nat. Phys. Sci.* **1973**, *20*, 20–22. [CrossRef]
36. Murata, K.; Kajiya, K.; Nukaga, M.; Suga, Y.; Watanabe, T.; Nakamura, N.; Ohno, H. A simple fabrication method for three-dimensional gold nanoparticle electrodes and their application to the study of the direct electrochemistry of cytochrome c. *Electroanalysis* **2010**, *22*, 185–190. [CrossRef]
37. Takeda, K.; Ishida, T.; Igarashi, K.; Samejima, M.; Nakamura, N.; Ohno, H. Effect of amines as activators on the alcohol-oxidizing activity of pyrroloquinoline quinone-dependent quinoprotein alcohol dehydrogenase. *Biosci. Biotechnol. Biochem.* **2014**, *78*, 1195–1198. [CrossRef] [PubMed]